Nuclear Magnetic Resonance (NMR)

Marcus Liebmann

II. Physikalisches Institut, RWTH Aachen

January 16, 2025

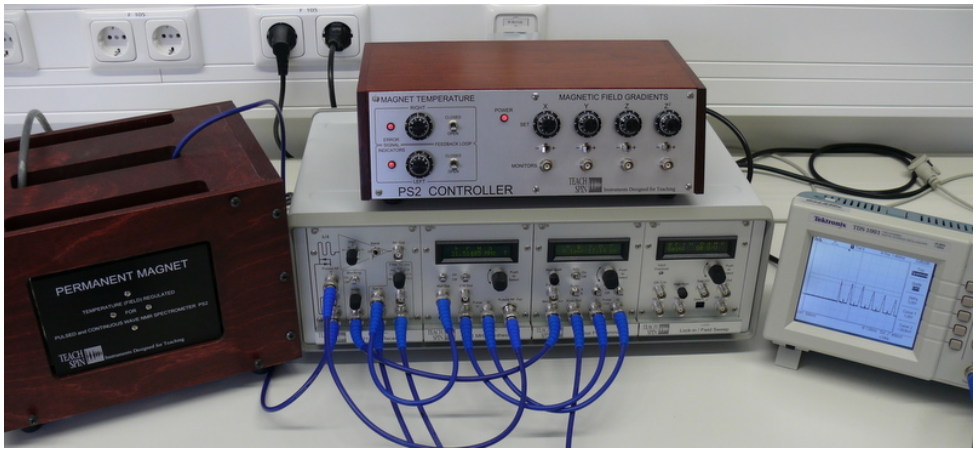

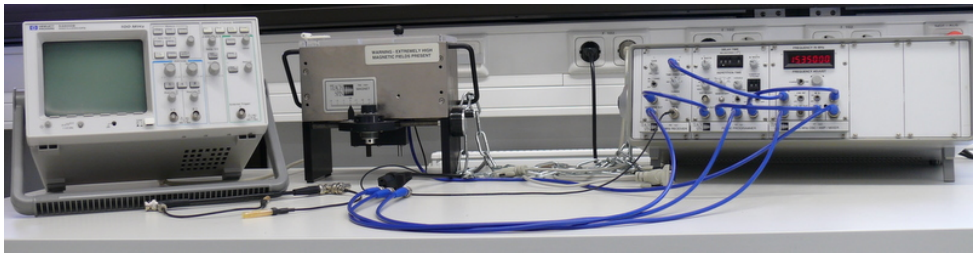

Contents

List of Figures

1 NMR - an overview

The beginnings of nuclear magnetic resonance spectroscopy (NMR) in the field of solid state physics go back to Edward Purcell and Felix Bloch in 1946. By placing samples, essentially consisting of nuclei with a magnetic moment, in a homogeneous, static magnetic field, they were able to observe the occurrence of resonances by irradiating and passing through the frequency of an electromagnetic field perpendicular to it. In most cases, a single coil serves as both the transmitting and receiving coils. This method of spectrum recording is called CW (Continuous Wave) and allows insights into the structure of complex binding states.

A further development of this method is the pulsed nuclear magnetic resonance spectroscopy (P-NMR) discovered by Erwin Hahn in 1950. Here, pulses are used instead of continuous irradiation.

By appropriate selection of duration and sequences of these pulses, new effects for analysis in the time domain could be found and specifically exploited, such as the **F**ree **I**nduction **D**ecay (FID) after one pulse or the so-called **Spinecho** after two or more pulses. Both phenomena will be discussed in more detail in the chapter 3. By means of the Fourier transform, the time signal recorded during P-NMR is converted into a spectrum. The advantage of the P-NMR method is a significantly better signal-to-noise ratio and a much shorter measurement time compared to the CW method.

Today's NMR spectrometers are based on the same basic principles and have become indispensable in modern physics and chemistry laboratories for the characterization of materials and structures. The NMR technique allows microscopic investigations of nuclei and their surroundings. In addition to its use in research, the concepts of NMR are also applied as an important medical imaging technique. To avoid the daunting term "nuclear", the term magnetic resonance imaging (MRI) is used synonymously.

How does such an image, e.g. of a human tissue structure, come about? For this purpose, it is exploited that different types of tissue have different relaxation and dephasing times. These are typical time constants of the nuclear spins after stimulation by an electromagnetic pulse irradiated from outside, presented in chapter 2.2. If these are measured spatially and transferred into a contrast image, very high resolution images, e.g. of human internal organs, can be obtained. This is done without the use of harmful radiation, which is a significant advantage over computed tomography (CT). Here, sections of the body image taken by means of radiation from different angles are combined to form a three-dimensional image.

Our experimental setup allows to apply the basic pulse techniques of NMR, to align magnetizations caused by the magnetic moments of the nuclear spins and to determine relaxation and dephasing times.

The concepts learned in the experiment can also be applied in a similar form to electron systems (electron spin resonance, or ESR). Especially the controlled alignment, manipulation and detection and the fundamental understanding of the dephasing and relaxation mechanisms of electron spins is the subject of current research in the field of quantum and spin electronics in solid-state physics. The driving forces of spin-based electronics are the *quantum computer* and the *spin transistor*.

The manifold applications of NMR techniques go, as indicated, far beyond this practical experiment. For the basics, the book by C. P. Slichter is recommended [1]. It is also worthwhile to have a look at the websites of research institutions and, in the medical field, at magnetic resonance images. Furthermore, many small applets can be found to illustrate pulse sequences in NMR.

2 Theoretical background

It is a good idea to treat the rather simple fact of the Zeeman splitting of a nucleus in an external magnetic field directly in quantum mechanical terms. The formalism in the Dirac notation and the repetition of some operator properties should not deter or push too much into the foreground at this point: The goal is to understand how the splitting and also the spin precession can be described and understood quantum mechanically.

2.1 Spin and magnetic moment

2.1.1 Quantum mechanical description of the spin precession

For this purpose we use the representation of the nuclear spin by the vector operator

$$\hat{\mathbf{S}} = (\hat{S}_x,\hat{S}_y,\hat{S}_z) \tag{1}$$

whose components contain the angular momentum operators for the individual spatial directions x, y and z. Let the z-direction be defined by an applied, constant magnetic field

$$\vec{B} = B_0 \cdot \hat{e}_z \tag{2}$$

The nucleons (protons and neutrons) that make up atomic nuclei are fermions and have half-integer spin. We now consider nuclei that have a non-zero total spin. In particular, we want to consider a hydrogen nucleus, i.e., a single proton, with spin $\frac{1}{2}$. For the component $\hat{S}_z$ and the vector operator $\hat{\mathbf{S}}$ the following eigenvalue equations hold:

$$\hat{S}_z \left|\uparrow\right\rangle = +\frac{\hbar}{2}\left|\uparrow\right\rangle, \tag{3}$$

$$\hat{S}_z \left|\downarrow\right\rangle = -\frac{\hbar}{2}\left|\downarrow\right\rangle, \tag{4}$$

$$\hat{\mathbf{S}}^2 \left|\uparrow\right\rangle = s(s+1)\left|\uparrow\right\rangle = \frac{3}{4}\hbar^2\left|\uparrow\right\rangle, \tag{5}$$

$$\hat{\mathbf{S}}^2 \left|\downarrow\right\rangle = s(s+1)\left|\downarrow\right\rangle = \frac{3}{4}\hbar^2\left|\downarrow\right\rangle. \tag{6}$$

Thus, the nuclear spin represents an ideal 2-level system with the energy states $|\uparrow\rangle$ und $|\downarrow\rangle$. These eigenstates span a 2D Hilbert space with orthonormal states:

$$\langle\uparrow|\downarrow\rangle = 0; \qquad \langle\uparrow|\uparrow\rangle = \langle\downarrow|\downarrow\rangle = 1; \tag{7}$$

and completeness relation:

$$\left|\uparrow\right\rangle\left\langle\uparrow\right| + \left|\downarrow\right\rangle\left\langle\downarrow\right| = \hat{1}. \tag{8}$$

A general spin operator, e.g. $\hat{S}_z$, thus has the matrix representation

$$\underline{\underline{S_z}} = \begin{pmatrix} \langle\uparrow|\hat{S}_z|\uparrow\rangle & \langle\uparrow|\hat{S}_z|\downarrow\rangle \\ \langle\downarrow|\hat{S}_z|\uparrow\rangle & \langle\downarrow|\hat{S}_z|\downarrow\rangle \end{pmatrix} = \frac{\hbar}{2}\begin{pmatrix} 1 & 0 \\ 0 & -1 \end{pmatrix} = \frac{\hbar}{2}\sigma_z. \tag{9}$$

Here, the Pauli matrix σ_z was introduced. Correspondingly, using ladder operators

$$\hat{S}_\pm = \hat{S}_x \pm i\hat{S}_y \tag{10}$$

with

$$\hat{S}_+\left|\uparrow\right\rangle = 0 \qquad \hat{S}_-\left|\uparrow\right\rangle = \hbar\left|\downarrow\right\rangle \tag{11}$$

$$\hat{S}_+\left|\downarrow\right\rangle = \hbar\left|\uparrow\right\rangle \qquad \hat{S}_-\left|\downarrow\right\rangle = 0 \tag{12}$$

it can be shown that also $\underline{\underline{S_x}}$ and $\underline{\underline{S_y}}$ can be represented in the same way using Pauli matrices:

$$\begin{aligned} \underline{\underline{S_x}} &= \frac{\hbar}{2}\begin{pmatrix} 0 & 1 \\ 1 & 0 \end{pmatrix} = \frac{\hbar}{2}\sigma_x \\ \underline{\underline{S_y}} &= \frac{\hbar}{2}\begin{pmatrix} 0 & -i \\ i & 0 \end{pmatrix} = \frac{\hbar}{2}\sigma_y \\ \underline{\underline{S_z}} &= \frac{\hbar}{2}\begin{pmatrix} 1 & 0 \\ 0 & -1 \end{pmatrix} = \frac{\hbar}{2}\sigma_z \end{aligned} \tag{13}$$

or shortly in vector notation:

$$\vec{S} = \frac{\hbar}{2}\vec{\sigma} \tag{14}$$

Assuming that the nucleus is stationary and not subjected to any external potential, a 2D Schrödinger equation (the so-called Pauli equation) can be formulated, which reduces to the interaction of the magnetic field with the spin:

$$i\hbar\frac{\partial}{\partial t}\left|s\right\rangle = -\frac{1}{2}g\mu_N\vec{\sigma}\cdot\vec{B}\left|s\right\rangle = -\frac{1}{2}g\mu_N\hat{\sigma}_z B_0\left|s\right\rangle \tag{15}$$

Here, $|s\rangle$ denotes the general spin state which is composed as a superposition of $|\uparrow\rangle$ and $|\downarrow\rangle$ with the corresponding time-dependent probability amplitudes $\alpha_+(t)$ and $\alpha_-(t)$.

$$|s\rangle = \alpha_+(t)\,|\uparrow\rangle + \alpha_-(t)\,|\downarrow\rangle \tag{16}$$

$$= a_+ \mathrm{e}^{-iE_\uparrow t/\hbar}\,|\uparrow\rangle + a_- \mathrm{e}^{-iE_\downarrow t/\hbar}\,|\downarrow\rangle\,. \tag{17}$$

This representation (17) inserted into the Pauli equation (15) yields the two energy eigenvalues:

$$E_\uparrow = -\frac{1}{2} g \mu_N B_0 = -\frac{1}{2}\hbar\gamma B_0 \tag{18}$$

$$E_\downarrow = \frac{1}{2} g \mu_N B_0 = \frac{1}{2}\hbar\gamma B_0 \tag{19}$$

With the nuclear magneton $\mu_N = e\hbar/2m_p$ and the gyromagnetic ratio

$$\gamma_{\mathrm{Proton}} = 2.675 \cdot 10^8 \,\frac{1}{\mathrm{T}\cdot\mathrm{s}}, \tag{20}$$

which links the spin to the magnetic moment:

$$\vec{\mu} = \gamma \vec{S}\,. \tag{21}$$

The spin component in the Pauli equation (15) thus causes the degeneracy to be lifted when the magnetic field is applied (Fig. 1).

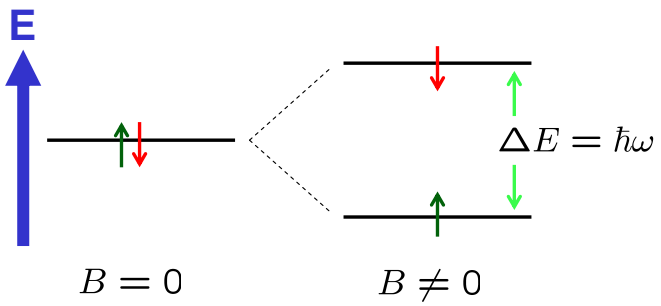

Figure 1: Lifting of spin degeneracy after switching on an external magnetic field B (Zeeman splitting) with energy eigenvalues $\mathrm{E}_\uparrow$ and $\mathrm{E}_\downarrow$.

The spin precession can now be expressed by calculation of the expectation values:

$$\langle \hat{S}_x \rangle = \frac{h}{2}\,\langle s \mid \hat{\sigma}_x \mid s \rangle = a_+ a_- \hbar \cos(\omega t) \tag{22}$$

$$\langle \hat{S}_y \rangle = \frac{h}{2}\,\langle s \mid \hat{\sigma}_y \mid s \rangle = a_+ a_- \hbar \sin(\omega t) \tag{23}$$

$$\langle \hat{S}_z \rangle = \frac{h}{2}\,\langle s \mid \hat{\sigma}_z \mid s \rangle = \frac{\hbar}{2}\left(|\alpha_+|^2 - |\alpha_-|^2\right) \tag{24}$$

Thus, the magnetic moment of the spin precesses about the external magnetic field (Fig. 2).

2.1.2 Simple resonance theory

The energy difference between the split levels from Eq. (18) and (19) amounts to

$$\Delta E = E_\downarrow - E_\uparrow = \hbar\gamma B_0. \tag{25}$$

With the help of photons of the energy

$$E_{\mathrm{Photon}} = \hbar \cdot \omega_L \stackrel{!}{=} \hbar \cdot \gamma B_0 \tag{26}$$

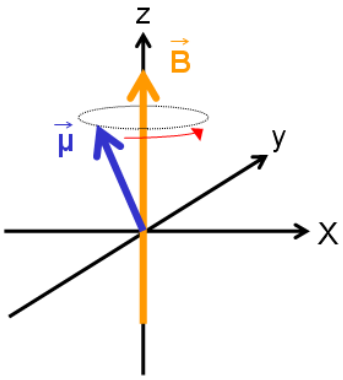

Figure 2: Classical representation of the precession of a magnetic moment μ about the static magnetic field in the z-direction.

a spin flip can be achieved. Here ω_L is the so-called Larmor frequency with which the spins precess around the magnetic field. We have thus shown that these spins can interact with an irradiated field of frequency ω_L. In NMR these frequencies are typically in the MHz frequency range (radio waves). The Larmor frequency or, equivalently, the magnitude of the splitting of the energy levels is directly proportional to the strength of the applied magnetic field, as it results directly from Eq. 26:

$$\omega_L = \gamma B_0 \tag{27}$$

2.2 Bloch equations

So far, a single spin or a single magnetic moment in the static magnetic field has been considered. However, we are looking for a macroscopic description of the time evolution of the magnetic moments of many nuclei. If we sum up the contributions of the single magnetic moments classically (here we abstain from an otherwise usual normalization to the volume), we obtain the magnetization:

$$\vec{M} = \sum_i \vec{\mu}_i \,. \tag{28}$$

Macroscopically, the equations of motion of the individual magnetization components, the Bloch equations, can then be formulated phenomenologically:

$$\frac{dM_x}{dt} = \gamma \left(\vec{M} \times \vec{B}\right)_x - \frac{M_x}{T_2} \tag{29}$$

$$\frac{dM_y}{dt} = \gamma \left(\vec{M} \times \vec{B}\right)_y - \frac{M_y}{T_2} \tag{30}$$

$$\frac{dM_z}{dt} = \gamma \left(\vec{M} \times \vec{B}\right)_z + \frac{M_0 - M_z}{T_1} \tag{31}$$

Here $M_0 = \chi_0 B_0$ denotes the equilibrium magnetization which is proportional to the magnetic field B_0 via the susceptibility χ_0. Obviously, the Bloch equations have a similar structure among themselves, since the temporal change of the magnetization components is composed in each case of two characteristic terms: on the one hand the precession of the magnetization around the applied magnetic field and on the other hand the relaxations with the characteristic times T_1 and T_2. The latter times describe how the system moves back to the equilibrium state after a perturbation, e.g. by an applied pulse. In thermal equilibrium, the transverse magnetizations M_x and M_y are zero. There is only one effective magnetization $M_z = M_0$ in the z direction.

The relaxations are caused by the following effects:

- Spin-lattice relaxation of the z component (T_1 relaxation time): The spin system interacts with the phonons of the lattice (absorption, emission, scattering). More generally, T_1 describes the energy relaxation of the system.

- Spin-spin relaxation (T_2 relaxation time): spins interact with each other, leading to relaxation.
- Diffusion of molecules in liquids.
- Other effects that are negligible at this point.

The spin-spin relaxation is included in T_2, but also the diffusion through molecules in liquids (which will be neglected here). The name spin-spin relaxation for T_2 is somewhat misleading, since this includes not only the relaxation due to the interaction of the spins with each other, but also the interaction of the spin system with the lattice, i.e. the phonons. Of course, the spin-lattice relaxation can only occur for the z component of the magnetization, since in the other two components the energy of the spin states is degenerate. Without an external magnetic field, the equilibrium magnetization is also zero in z direction ($M_0 = 0$). Furthermore, a distinction between T_1 and T_2 is no longer meaningful, since all magnetization directions are energetically equal. In this case, the Bloch equations look the same in all three components.

The Bloch equations are solved by transforming into a rotating system of reference. Let the system S' rotate with the angular velocity $\vec{\omega}$ with respect to the fixed laboratory system S. Consider a function $\vec{F} = F_{x'} \cdot \hat{e}_{x'} + F_{y'} \cdot \hat{e}_{y'} + F_{z'} \cdot \hat{e}_{z'}$ in the system S'. For the unit vectors:

$$\frac{d\hat{e}_{i'}}{dt} = \vec{\omega} \times \hat{e}_{i'} \tag{32}$$

This gives for the time derivative of the function $\vec{F}$:

$$\begin{aligned}
\frac{d\vec{F}}{dt} &= \frac{dF_{x'}}{dt} \cdot \hat{e}_{x'} + F_{x'} \cdot \frac{d\hat{e}_{x'}}{dt} + \frac{dF_{y'}}{dt} \cdot \hat{e}_{y'} + F_{y'} \cdot \frac{d\hat{e}_{y'}}{dt} + \frac{dF_{z'}}{dt} \cdot \hat{e}_{z'} + F_{z'} \cdot \frac{d\hat{e}_{z'}}{dt} \\
&= \frac{dF_{x'}}{dt} \cdot \hat{e}_{x'} + \frac{dF_{y'}}{dt} \cdot \hat{e}_{y'} + \frac{dF_{z'}}{dt} \cdot \hat{e}_{z'} + \vec{\omega} \times \vec{F} \\
&= \frac{\partial \vec{F}}{\partial t} + \vec{\omega} \times \vec{F}
\end{aligned} \tag{33}$$

We will use this general relation in the next section.

2.3 Alternating field in the rotating reference system

A single magnetic moment $\vec{\mu}$ precesses about an applied magnetic field $\vec{B}$:

$$\frac{d\vec{\mu}}{dt} = \vec{\mu} \times \gamma \vec{B} \tag{34}$$

According to Eq. 33, the equation of motion for $\vec{\mu}$ in a frame of reference rotating with the same frequency as the precession ω is:

$$\frac{\partial \vec{\mu}}{\partial t} + \vec{\omega} \times \vec{\mu} = \vec{\mu} \times \gamma \vec{B} \tag{35}$$

$$\frac{\partial \vec{\mu}}{\partial t} = \vec{\mu} \times \gamma \left(\vec{B} + \frac{\vec{\omega}}{\gamma} \right) \tag{36}$$

We thus obtain an effective magnetic field $\vec{B}_{\text{eff}}$ around which the magnetic moments precess:

$$\vec{B}_{\text{eff}} = \vec{B} + \frac{\vec{\omega}}{\gamma} \tag{37}$$

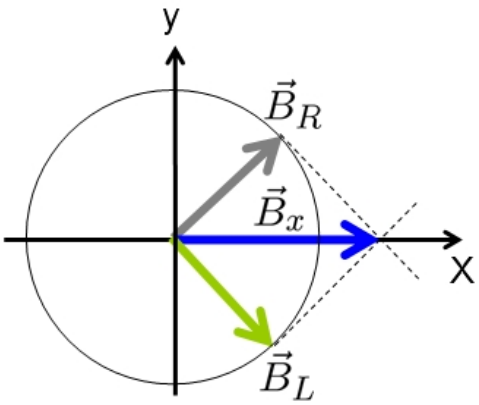

Figure 3: Decomposition of the periodic alternating field into right and left circulating fields.

For a periodically changing magnetic field in the x direction of the laboratory system $\vec{B}_S = 2B_1 \cdot \cos\omega_p t \cdot \hat{e}_x$, we can perform a decomposition $\vec{B}_S = \vec{B}_R + \vec{B}_L$ into two circular fields in the xy plane (Fig. 3):

$$\vec{B}_R = B_1 \left(\cos\left(\omega_p t\right) \cdot \hat{e}_x + \sin\left(\omega_p t\right) \cdot \hat{e}_y\right) \tag{38}$$

$$\vec{B}_L = B_1 \left(\cos\left(\omega_p t\right) \cdot \hat{e}_x - \sin\left(\omega_p t\right) \cdot \hat{e}_y\right) \tag{39}$$

This field can now be used to induce a spin flip as described in Section 2.1.2. For this, of course, the frequency ω_p must correspond to the Larmor frequency ω_L.

A photon is a massless spin 1 particle, so it can take the values $m_z = \pm 1$. The setting of the spins corresponds to the polarization direction of the irradiated photons. After the following consideration of the conservation of angular momentum and energy, this leads to an important conclusion. Because of the conservation of angular momentum, the sum of the two spins of the nucleus and the photon must be the same before and after the process. Therefore, we investigate the different combinations of nuclear and photon spin setting (Tab. 1).

Initial state		Final state		
nucleus	photon	nucleus	photon	
$+\frac{1}{2}$	+1	$+\frac{1}{2}$	+1	no interaction
$+\frac{1}{2}$	-1	$-\frac{1}{2}$	–	photon absorbed
$-\frac{1}{2}$	+1	$-\frac{1}{2}$	+1	no interaction
$-\frac{1}{2}$	-1	$+\frac{1}{2}$	-1,-1	photon emitted

Table 1: Interaction possibilities when combining different nuclear and photon spin settings.

In the first case, no interaction can take place because the nucleus cannot assume a spin setting of $+\frac{3}{2}$, but also cannot emit a photon because it is already in the lowest-energy state. In the second case, the photon is absorbed and the nuclear spin flips to the energetically higher state. The third case allows no absorption of the photon, since it is in the energetically higher state, but also no emission can take place, since the conservation of momentum would be violated. The fourth case finally represents the induced emission. The nuclear spin flips and emits, excited by the incident photon, another photon and thereby goes into the energetically lower state. Thus, only the photons with the spin -1 can act. Since the polarization of the photons is related to their spin setting as mentioned above, only one of the two fields obtained in the decomposition is effective. The other one has no effect on the spin system and therefore will not be considered in the further course.

Thus, applying this additional alternating field in x direction, we obtain a field acting on the spins:

$$\vec{B}_{\text{ges}} = \vec{B}_0 + \vec{B}_1 = \begin{pmatrix} B_1 \cos \omega_p t \\ -B_1 \sin \omega_p t \\ B_0 \end{pmatrix} \tag{40}$$

where we denote with $\vec{B}_0$ the magnitude of the static $\vec{B}$ field according to Eq. 2. The magnetic moments then precess about the total field $\vec{B}_{\text{ges}}$ according to the equation of motion:

$$\frac{d\vec{\mu}}{dt} = \vec{\mu} \times \gamma \left(\vec{B}_0 + \vec{B}_1 \right) \tag{41}$$

Let us now switch to a frame of reference rotating with frequency $\omega_z = -\omega_p$ about the z axis. According to Eq. 36, we obtain:

$$\frac{\partial \vec{\mu}}{\partial t} = \vec{\mu} \times \left((\omega_z + \gamma B_0)\, \hat{e}_z + \gamma B_1 \hat{e}_{x'} \right) \tag{42}$$

$$= \vec{\mu} \times \gamma \left(\left(B_0 - \frac{\omega_p}{\gamma} \right) \hat{e}_z + B_1 \hat{e}_{x'} \right) = \vec{\mu} \times \gamma \vec{B}_{\text{eff}} \tag{43}$$

with the effective magnetic field

$$\vec{B}_{\text{eff}} = B_1 \hat{e}_{x'} + \left(B_0 - \frac{\omega_p}{\gamma} \right) \hat{e}_z \,. \tag{44}$$

In this form of the effective field, the effect of the irradiation with the oscillating field with frequency ω_p can be understood: in z direction the static field is opposed by a partial component of the alternating field (Fig. 4).

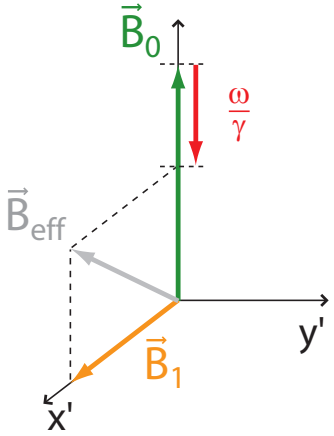

Figure 4: Effective magnetic field. In the rotating reference frame the static field B_0 in z direction is reduced by the amount $\frac{\omega}{\gamma}$ and disappears completely in case of rotation with the Larmor frequency ω_{L}.

In the resonance case, where the frequency of the irradiated alternating field just corresponds to the Larmor frequency, i.e. $\omega_p = \gamma B_0 = \omega_L$, the alternating field can even completely compensate the external field in z direction: then only the component in the x' direction remains in the rotating system. The magnetic moments then precess about the x' axis. The following step is decisive: if we apply the alternating field in x' direction for a certain time $T_{2\pi}$, the magnetization precesses exactly once around the x' axis. Accordingly, for a set irradiation time of $T_{\pi/2}$, the magnetic moments are rotated from the z direction to the y' direction, as Fig. 5 shows. We have thus found a way to rotate the magnetic moments, and thus the magnetization as a macroscopically measurable quantity, into the xy plane or into the $-z$ direction, for example, and to align them in a specific direction.

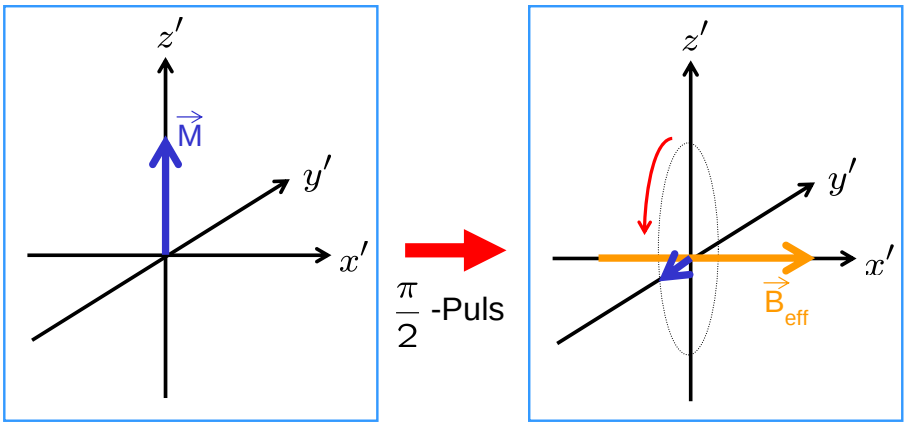

Figure 5: The magnetization can be selectively rotated by $\pi/2$ by irradiating a resonant alternating field pulse of length $T_{\pi/2}$, which causes an effective B field in the x' direction.

What does this movement now look like in the fixed laboratory frame S? While the field $\vec{B}_1$ is applied, the magnetic moments precess around the effective magnetic field $\vec{B}_{\text{eff}}$; without this field they rest in the moving reference frame S'. However, S' rotates in the laboratory system S, so the magnetic moments precess in the xy plane of S. The magnetization is now again the sum of the individual magnetic moments. Thus, the magnetization also precesses about the z axis, producing a magnetic flux. If we now attach a coil in the xy plane of the laboratory system, we can measure a voltage proportional to the magnetic flux and thus proportional to the magnetization, due to Faraday's law. Of course, this is only the case as long as there is a fixed phase relation between the motions of the individual magnetic moments. However, as we will see later, this is not always the case.

So, in summary, with the help of the additional irradiation of the RF field, we have the possibility to flip the magnetization out of the thermodynamic equilibrium (z direction) and to measure the magnetization in the xy plane with the help of the coil. This realizes the so-called P-NMR (Pulsed-NMR) technique.

3 P-NMR and the generation of FIDs

In the last chapter we saw that with the help of an alternating field the magnetization can be flipped out of thermal equilibrium in different directions. So what does the pulse look like that we can record using the coil? We apply a so-called $\pi/2$ pulse. This has length $T_{\pi/2}$ and rotates the magnetization from the $+z$ direction to the y' direction. Thus, in the laboratory system, the magnetization precesses around the z axis. On the oscilloscope, a high narrow pulse (the $\pi/2$ pulse) can be seen followed by an exponentially decreasing peak.

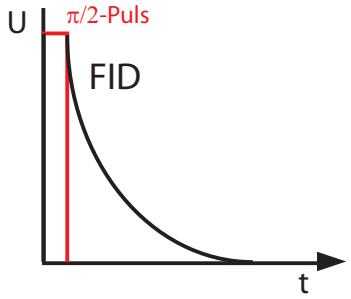

Figure 6: Image of the voltage U induced in the measuring coil after applying a $\pi/2$ pulse. An exponential drop, a so-called Free Induction Signal (FID) signal, can be seen.

This falling peak is a measure of magnetization and is called "free induction decay" (FID). There are two reasons for the decrease in magnetization. As we noted above, the x and y components of the magnetization relax with time T_2. Therefore, one should be able to extract the relaxation time T_2 from this signal. However, inhomogeneities of the magnetic field also come into play, so that the unambiguous determination of T_2 is not possible. The inhomogeneities cause the Larmor frequencies to vary slightly depending on the location within the sample, and therefore some magnetic moments precess faster and some slower than the rest. This leads to a weakening of the phase relation of the motions of the individual magnetic moments and therefore to a reduction in magnetization. Depending on which effect is stronger, the signal is determined by the inhomogeneities in the magnetic field or the spin-spin relaxation.

4 Determination of the longitudinal and transverse relaxation time

4.1 Spin-lattice relaxation time T_1

But how can we still determine the relaxation times from the pulses? To do this, we will first take a closer look at the determination of T_1. The aim is to determine the relaxation of the magnetization in z direction. First, we apply a π pulse to the sample. Thereby we rotate the magnetization from the $+z$ direction into the $-z$ direction. On the oscilloscope, of course, only the pulse itself can be seen, but no FID, since the magnetization is perpendicular to the xy plane and therefore cannot be recorded with the coil (Fig. 7).

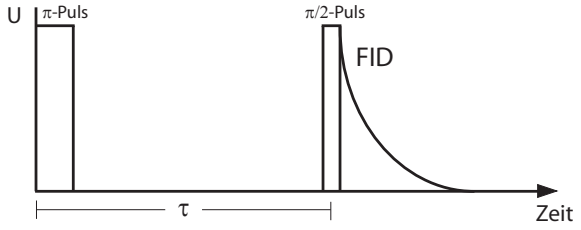

Figure 7: Pulse sequence for determining T_1 on the oscilloscope.

Now we let the relaxation run undisturbed for a period of τ and then want to measure the remaining magnetization. But since we can only do this in the xy plane, we apply a $\pi/2$ pulse to the sample system and then look at the height of the resulting FID. So we apply the pulse sequence $\pi \to \tau \to \pi/2$, as summarized in Fig. 8.

The behavior of the magnetization in the z direction can be derived relatively easily. From the Bloch equations it follows under the initial condition that the magnetization in thermal equilibrium is M_0 and the magnetization present at the beginning of the relaxation is $M(0)$:

$$M_z(t) - M_0 = (M(0) - M_0) \cdot e^{-\frac{t}{T_1}} \tag{45}$$

In our case, $M(0) = -M_0$, since we directly rotate into the $-z$ direction, yielding (Fig. 9):

$$M_z(t) = M_0 \left(1 - 2 \cdot e^{-\frac{t}{T_1}}\right) \tag{46}$$

A quick estimation for T_1 is obtained via the so-called "zero-crossing-point". This is the intermediate situation during the course of relaxation when the total magnetization vanishes. A simple relation between the time τ_0 of the zero crossing and T_1 can then be derived from Eq. (46):

$$T_1 = \frac{\tau_0}{\ln 2} \tag{47}$$

To determine the relaxation time T_2, one makes use of an interesting spin effect, which we will discuss below.

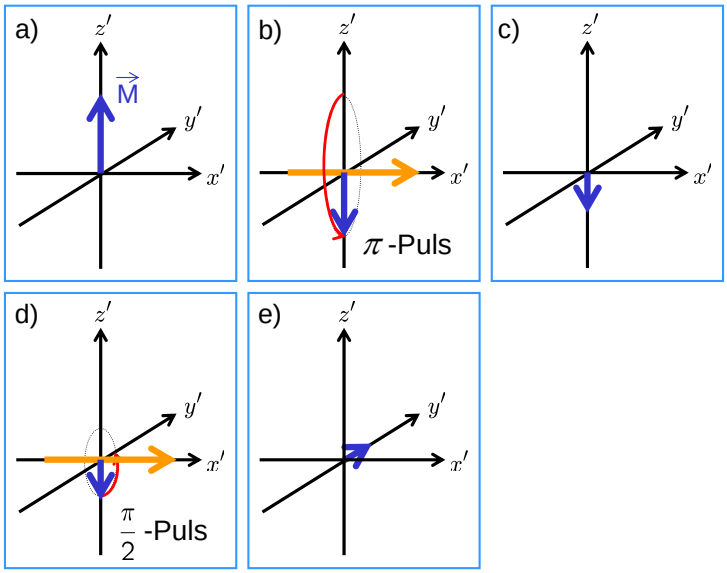

Figure 8: Evolution of the magnetization during the pulse sequence to determine T_1. (a) Initial state: The net magnetization $\vec{M}$ points in the direction of the static magnetic field. (b) By applying a π pulse, the magnetization can be flipped in the opposite direction. (c) After waiting for a time τ, some spins are relaxed so that the net magnetization decreases in magnitude. (d) By means of a $\frac{\pi}{2}$ pulse, the magnetization can finally be rotated into the xy plane. (e) In this plane it can now be detected.

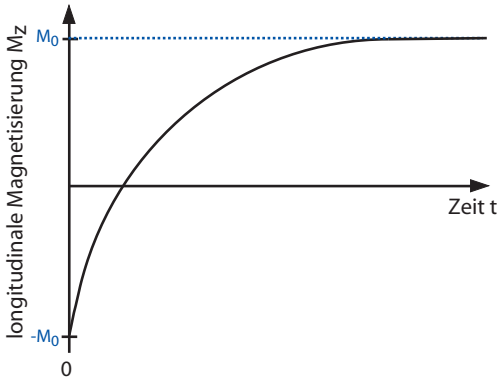

Figure 9: Time dependence of the longitudinal magnetization M_z.

4.2 Spin-spin relaxation time T_2

We now want to measure the relaxation in the xy plane by applying a pulse sequence as shown in Figure 10. We first flip the magnetization into the xy plane with a $\pi/2$-pulse. Then we wait a time τ in which the relaxation can proceed undisturbed. Now the effect due to the inhomogeneities of the magnetic field occurs, which we discussed above. After the waiting time τ, just a part δM of the magnetization has shifted by the angle $\delta\phi$ with respect to the other magnetic moments. Here $\delta\phi$ is positive if δM precesses faster than the average and negative if δM is slower than the average. Now we apply a π pulse to the system. By doing this, we achieve that the $\delta\phi$ are inverted. After another time τ, δM has again traveled an angle $\delta\phi$, however, by inverting the angles before, we have achieved that the summation of these two angles now gives 0 and the phase relation of the individual magnetic moments are restored. Therefore, an echo pulse appears on the oscilloscope as shown in Fig. 11.

By varying τ we can now record a curve from which we can then determine T_2. For the relaxation of the magnetization in xy-direction we get a simple exponential decay from the Bloch equations:

$$M_{xy}(t) = M_{x,y}(0) \cdot e^{-\frac{t}{T_2}} \tag{48}$$

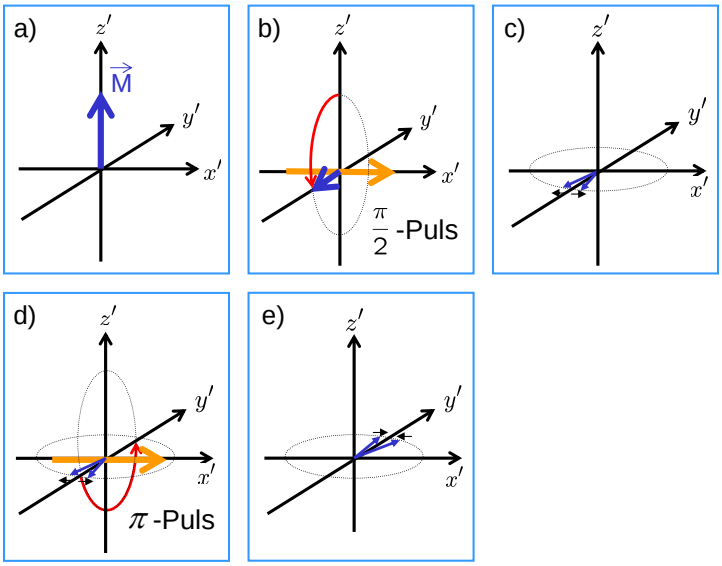

Figure 10: Evolution of the magnetization during the determination of T_2. (a) Initial situation: the net magnetization $\vec{M}$ is aligned along the z direction of the static magnetic field. (b) By applying a $\frac{\pi}{2}$ pulse, the magnetization can be rotated into the $x'y'$ plane. (c) During the time τ, dephasing of the spins takes place. There are faster and slower preceding parts, and the net magnetization smears. (d) By means of a π pulse, the spins are now flipped from one side of the $x'y'$ plane to the other. The immediate consequence is that after (d), the direction of the precessing parts is inverted. (e) The fanned-out magnetization is thus recombined, and a spin echo can be observed after time 2τ.

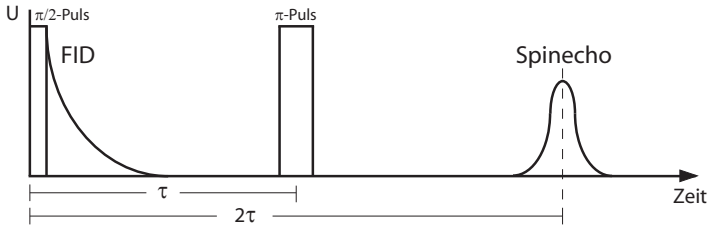

Figure 11: Pulse sequence for determination of T_2 on the oscilloscope.

In our case, $M_{x,y}(0)$ is again M_0. Graphically, then, the magnetization shows an exponential behavior (Fig. 12).

4.3 Optimization of the pulse sequence for the determination of T_2

4.3.1 The Carr-Purcell pulse sequence

Carr and Purcell developed a pulse sequence which is an extension to the conventional series of measurements for determining the T_2 relaxation time by measuring the spin echo while varying the delay time τ [2]. The decisive advantage is that the diffusion, which has not been taken into account so far and which affects the magnetization as follows, is no longer of importance:

$$M(2\tau) = M(0) \cdot e^{-\frac{2\tau}{T_2}} \cdot e^{-\left(\gamma \frac{\partial B}{\partial z}\right)^2 \frac{2}{3} D\tau^3} \tag{49}$$

Incidentally, it can be seen from this form that with known magnetic field gradients, the diffusion constant of the sample can also be determined. But what is the new idea in the Carr-Purcell method? Here, after the initial $\pi/2$ pulse at times τ, 3τ, 5τ, ... a π pulse is repeatedly applied. Then, after the

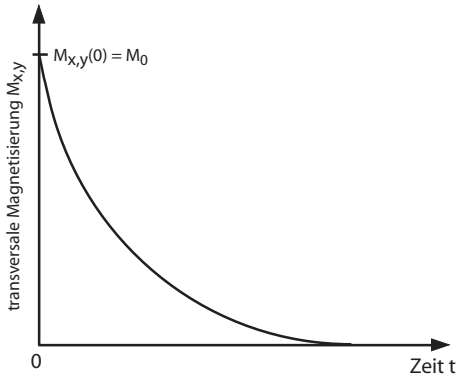

Figure 12: Transversal magnetization M_{xy} vs. time.

times 2τ, 4τ, 6τ, ... renewed spin echoes. So a fixed delay time τ is set. The variation of the time comes from considering the magnetization decrease of the spin echoes at the multiples of τ. The pulse sequence is shown schematically in Figure 13. For detailed understanding, we now go through it step by step.

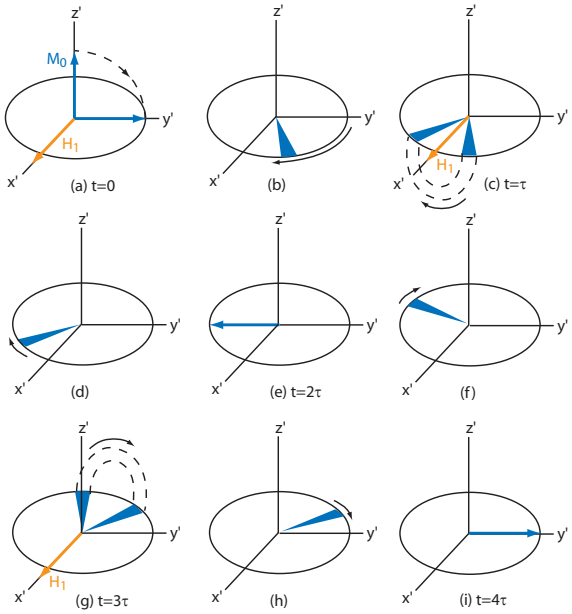

Figure 13: Carr-Purcell method, modified after [2]. Note that the rotating reference frame is shown here. (a) The sequence is initiated by a $\pi/2$ pulse that rotates the magnetization about the x' axis in the y' direction. The change in mean magnetization, shown by the arrow in (b), results from a frequency ω_{L} not perfectly tuned to ω_{p}. The π pulse after time τ folds the faster-preceding components to the far end of the shaded region (c), so that they catch up with the slower ones (d) and overlap with them after time 2τ to form a spin echo (e). In (f), the process starts again on the negative x' side. This alternating sequence accumulates any error in the length of the π pulse.

First, the initial magnetization due to the static field is rotated into the plane by irradiation with a $\pi/2$ alternating field pulse whose effective magnetic field (H_1 is used here synonymously with B_1, true to the original publication) points in the x' direction, see Fig. 13(a). During the delay time τ, the net magnetization vector in the laboratory system will be precessed by the angle $\theta = \tau(\gamma B_1 - \omega_p)$. Let the RF angular frequency of the alternating field pulse be denoted here by ω_p. Due to the inhomogeneities of B_0, the magnetization vectors of different volume elements precess at different rates. This fanning out behavior is indicated in Fig. 13(b) by the shaded region instead of a well-defined vector. Now

the first π pulse occurs without phase shift. Transferred to the rotating reference frame, this also generates an effective magnetic field in the x' direction. The fanned magnetization ends up in the xy-plane again at ideal setting of the π-pulse, as shown in Fig. 13(c). Now the net magnetization vector continues to precess within the next delay time τ (Fig. 13(d)). The inversion of the slow versus the fast components in the π pulse results in a spin echo just after a time $t = 2\tau$, as explained in section 4.2, since here the components are recombined, see Fig. 13(e). In Fig. 13(f), the process begins anew: the net magnetization precesses, and the spin components fan out due to the slightly different B-field strengths in the individual volume elements. Ideal in-plane flipping inverts the situation in Fig. 13(g), so that after another precession waiting time τ, shown in Fig. 13(h), the faster and slower precessing parts are merged in a spin echo at $t = 4\tau$, see Fig.13(i).

However, the Carr-Purcell pulse sequence has a decisive disadvantage: we cannot set the length of the π pulses as precisely as would be necessary. Therefore, each time the π pulse is applied, the deviation from the xy plane becomes successively larger.

4.3.2 The Meiboom-Gill pulse sequence

There are several approaches to avoid the accumulation of the deviation. In the Meiboom-Gill method [3], named after its inventors, the same pulse sequence is used as in the Carr-Purcell pulse sequence, where the irradiation of the RF alternating field to generate a π pulse is phase-shifted by 90° with respect to the field used in the original $\pi/2$ pulse. In the image of the rotating reference system, this means that the effective magnetic field points in a different axial direction. Let's look at the effect in detail: First, according to Fig. 14(a), we flip the initial magnetization about the y' axis into the xy plane (x' direction), where the precession and the fanning that takes place during the waiting τ, Fig. 14(a), can occur undisturbed. Now the π pulse is applied by the 90° phase-shifted alternating field and thus the magnetization is flipped about another axis (here x') in the plane, cf. Fig. 14(c), with the effect that after $t = 2\tau$ the spin echo occurs and the system is again in the same state as after application of the initial $\pi/2$ pulse. If the π pulse now does not ideally lead to the plane, the flap on the next pass does not point in the same direction as in the Carr-Purcell sequence, but cancels the error by flipping in practically the opposite direction.

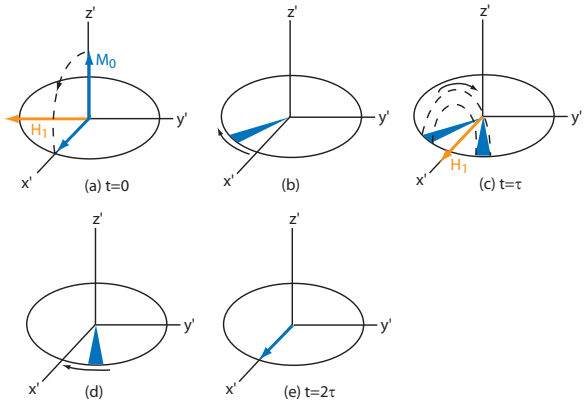

Figure 14: Meiboom-Gill method, modified after [3]. Due to the phase shift of the $\pi/2$-pulse, the magnetization of the π-pulse in the rotating frame of reference is shifted around the axis in which the magnetization was folded by the $\pi/2$-pulse at the beginning. An error in the length of the π-pulses does not accumulate but is cancelled after every second pulse.

5 Setup

Two almost identical NMR spectrometers are available in the lab course. The constant magnetic field $\vec{B}_0$ is generated by means of a permanent magnet. This magnet is relatively sensitive due to the materials used (rare earths). Therefore, it should be handled with appropriate care. Furthermore, care must be taken that no objects enter the sample chamber, as these would impair the homogeneity of the magnet. In the first setup, the alternating field is applied via two Helmholtz coils which act perpendicular to the field of the permanent magnet. The magnetization is picked up by a solenoid coil wound around the specimen holder, see Fig. 15. In the second experimental setup, the solenoid coil is used as both a transmitting and receiving coil. The Helmholtz coils are omitted here.

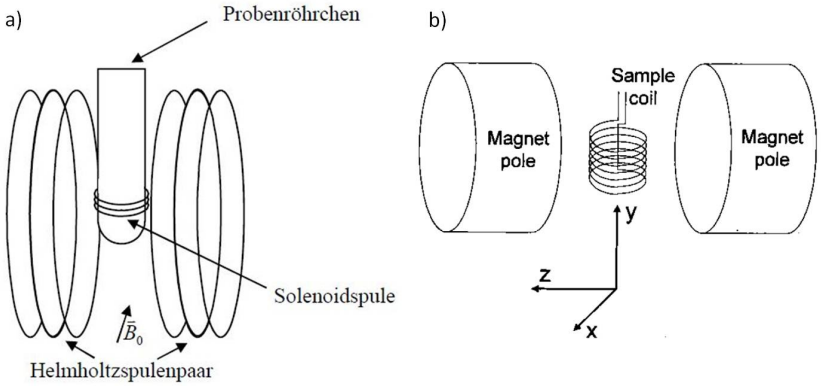

Figure 15: Geometry of the two experimental setups: Direction of the constant magnetic field (permanent magnet, B_0), the alternating field (Helmholtz coil pair), and the solenoid coil wound around the sample chamber as pick-up coil (a) and transmitting and receiving coil (b), respectively.

The individual modules of the spectrometer and their interconnection are shown schematically in Fig. 16.

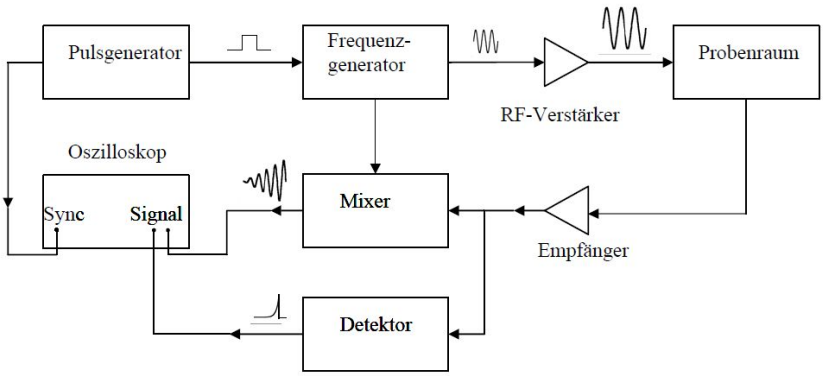

Figure 16: Layout diagram of the individual elements of the NMR spectrometer.

- The **amplifier** (Fig. 17) is connected directly to the receiving coil and has two outputs. One outputs a signal proportional to the amplitude of the AC voltage generated in the receiving coil by the precession of the magnetization. The second outputs a signal produced by multiplying the coil signal by that of the frequency generator. This can be used to match the frequency of the radiated signal with the Larmor frequency. Furthermore, it has another function called blanking. This is where the amplifier is switched to zero while the RF pulses are applied. In certain situations this can increase the clarity of the pulses on the oscilloscope, especially when longer pulse trains are present as in the Carr-Purcell or Meiboom-Gill method.

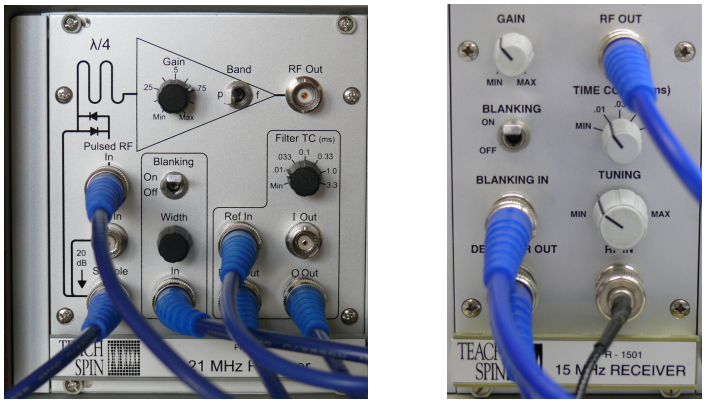

Figure 17: The amplifier units of the NMR spectrometers 1 and 2.

- The **pulse generator** (Fig. 18) is used to control the individual RF pulses. Via "A-width" and "B-width" the pulse durations can be set. Thus the π and $\pi/2$ pulses etc. can be set. Furthermore, the "delay time", or τ, i.e. the delay between the A-pulse and the B-pulse can be set. A delay of 2τ is built in between two consecutive B pulses to allow time for the spin echo. The "repetition" time gives the repetition rate of a pulse train, corresponding to the repetition period P. The setting "number of B-pulses" or N can be used to specify how many B-pulses should be given to the system after an A-pulse. This is important for the method according to Carr-Purcell and Meiboom-Gill. The pulses themselves can be turned on by the underlying A and B switches. The switch "sync" indicates which pulse should be selected as synchronization for the trigger of the oscilloscope. The output "sync out" should be connected to the trigger input of the oscilloscope.

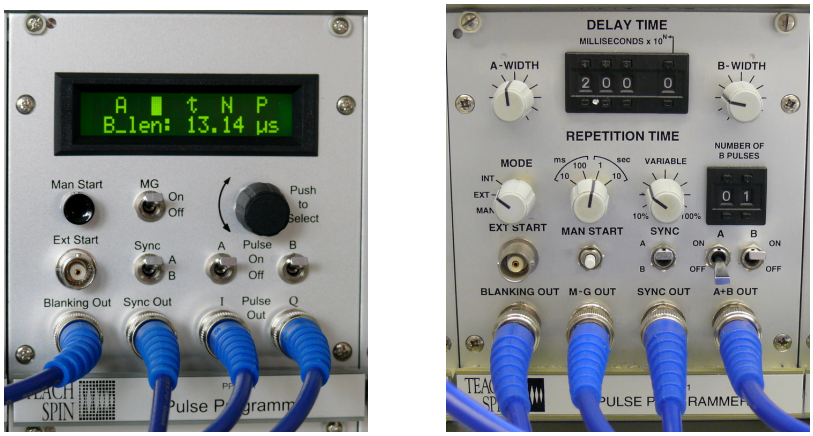

Figure 18: The pulse generators. Here the essential settings for the pulse sequences are made: the lengths of the A and B pulses, the waiting time τ between the pulses, the number of B pulses N and the period P of the entire pulse sequence.

- The **frequency generator** (Fig. 19) sends the radio frequency signal to the transmitting coils. The individual pulses are controlled with the pulse generator. The frequency can be adjusted via the "frequency adjust" control, with the switch next to it reflecting the fine or coarse setting. The switch M-G indicates whether or not the RF signal of the A pulse should shift by 90° against that of the B pulse. If this switch is on, then the measurement can be performed according to the method of Meiboom-Gill. In this slot there is a second device, the mixer. With its help it is possible to make a Fourier analysis of the obtained signal and adjust the frequency to the Larmor frequency. **Important:** The frequency generator must never be operated without

connection to the transmitting coil (the screwable connection), otherwise it can be damaged!

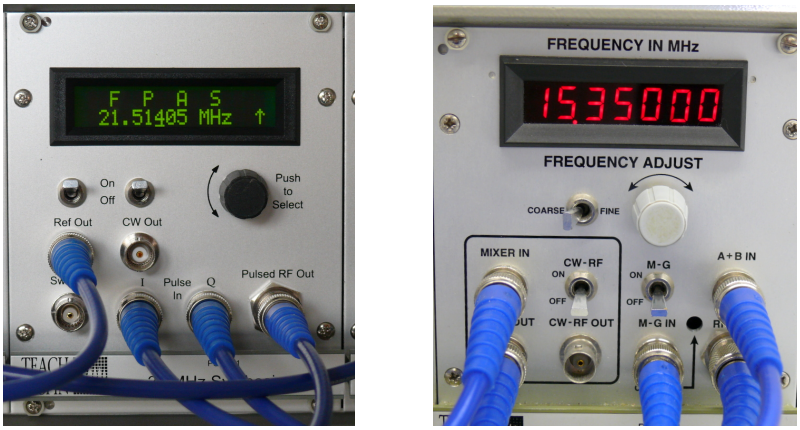

Figure 19: The frequency generators. This is where the resonant frequency is set.

- The pulse sequences are displayed on an **oscilloscope**. Horizontal and vertical cursors can be used to simplify the reading of pulse heights and lengths. Likewise, the oscilloscope has an external trigger input that allows synchronization of the oscilloscope image to the start of the A or B pulse.

6 Experimental procedure and tasks

The relaxation times T_1 and T_2 of hydrogen nuclei in a mineral oil sample are to be determined with the presented pulse sequences. In order to perform the measurements, a prior adjustment of the relevant parameters is necessary.

6.1 Preliminary test conductor loop

In order to estimate the required pulse lengths, it is first necessary to know the strength of the irradiated alternating field. A conductor loop is attached to each experiment (Fig. 20).

Figure 20: Conductor loop for direct measurement of the RF pulses. It can be fixed in height with the help of the rubber ring.

This small measuring coil has a cross-sectional area A. With it we can determine the strength of the RF alternating field. For this purpose, the loop is inserted with the opening in the y direction, i.e. parallel to the Helmholtz coil pairs or, in the case of the second setup, in the direction of the transmitting coil. The socket of the coaxial cable is clamped to the connector, which is fitted with a resistor to negate the effects of the cable, and then connected to an input of the oscilloscope via another cable. The pulse generator is now used to control the alternating field. For this purpose an A pulse is applied and the repetition rate or pulse sequence period is chosen sensibly. Of course the output "sync out" must be connected to the trigger input of the oscilloscope. On the oscilloscope the alternating field should be visible if the time constant and the y resolution are chosen correctly. Faraday's law can then be used to determine the strength of the field:

$$U = -\frac{d\Phi}{dt} = -\frac{d}{dt}\int \vec{B}_s \cdot \vec{df} \tag{50}$$

where U denotes the voltage induced in the conductor loop, Φ the magnetic flux, and $\vec{df}$ a vector surface element. $\vec{B}_s$ is the linearly polarized alternating field generated by the transmitting coil. However, only one of the two circularly polarized components is responsible for the manipulation of the spins (see Sect. 2.3). $\vec{B}_s$ now has the form:

$$\vec{B}_s = B_1 \left(\cos \omega_p t \cdot \hat{e}_x + \sin \omega_p t \cdot \hat{e}_y\right) + B_1 \left(\cos \omega_p t \cdot \hat{e}_x - \sin \omega_p t \cdot \hat{e}_y\right) \tag{51}$$

$$= 2B_1 \cos \omega_p t \cdot \hat{e}_x \tag{52}$$

Here ω_p is the angular frequency of the applied field. However, the display of the frequency generator shows the actual frequency and not the angular frequency, so that the value must still be provided with the factor 2π. Since the receiver loop (N turns) should be set so that the aperture is perpendicular to the field, Eq. 50 with Eq. 52 yields

$$U = 2B_1 \omega_p \sin \omega_p t \cdot N \cdot A = U_0 \sin \omega_p t \tag{53}$$

$$B_1 = \frac{U_0}{2\omega_p N A} \tag{54}$$

From this, the time duration of a $\pi/2$ pulse is now to be determined. From the theoretical considerations we know that in the time $2\pi/\omega_L'$ a complete rotation of the magnetic moments around the x' axis can be generated. (Note: ω_L' is not to be confused with the precession frequency ω_L, around the static B-field!) So a $\pi/2$ pulse takes the time

$$T_{\pi/2} = \frac{\pi}{2} \cdot \frac{1}{\omega_L'} = \frac{\pi}{2\omega_L'} \,. \tag{55}$$

On the other hand, it is obtained from Eq. 27 that the relation $\omega_L' = \gamma B_1$ holds, so in total:

$$T_{\pi/2} = \frac{\pi}{2\gamma B_1} = \frac{\pi N A \omega_p}{\gamma U_0}. \tag{56}$$

This pulse duration is then set with "A-width" on the pulse generator.

6.2 Settings optimization

So the corresponding pulse should be present, which gives us the maximum FID at the given frequency, because the magnetization (within the scope of the only approximated resonance frequency) was folded into the xy plane. Based on this FID, the amplifier setting is now made. To do this, the conductor loop is removed and the sample tube containing the mineral oil is placed in the sample chamber. The gain is optimized so that a good signal-to-noise ratio prevails. The time scale and y resolution on the oscilloscope is chosen accordingly, the *repetition time* is set to around one second and the tuning, i.e. the frequency dependent gain is adjusted so that the FID is maximized.

After the basic setting of the amplifier, the so-called sweet spot must be searched for and the correct resonance frequency must be set. The sweet spot is the point of maximum homogeneity of the magnetic field. The adjustment of the sweet spot and the resonance frequency must be done simultaneously, because the resonance frequency depends on the magnetic field. The resonant frequency can be optimized via the Fourier signal. The Fourier signal can be taken from the second amplifier output coming from the mixer. This is obtained by multiplying the AC voltage picked up by the coil (frequency ω_L) by the AC voltage irradiated from outside (frequency ω_p). According to the addition theorem, the result is a beating pattern:

$$2 \cos \omega_L t \cdot \cos \omega_p t = \cos \left(\omega_L + \omega_p\right) t + \cos \left(\omega_L - \omega_p\right) t \,. \tag{57}$$

Only the low frequency part $\propto \cos \left(\omega_L - \omega_p\right) t$ appears at the output. The signal visible there should have no more beatings. If the beats look rather deformed, it may be because the sample is not in the

sweet spot. In many cases it is sufficient to vary the height of the sample by means of the rubber ring to the position adjustment in order to find the optimal position. However, the displacements should not be particularly large. It should be noted that the duration of the various pulses is frequency dependent and these must be adjusted accordingly by hand. So in order to get the FID at maximum and to be able to make the adjustment accordingly well, the length of the A-pulse must also be readjusted.

After an optimal FID has been found, a first estimate for T_1 can now be made. For this purpose, the *repetition time* is turned down until the FID has about one third of the maximum value. The decrease in magnetization can be explained by the fact that thermal equilibrium can no longer be established before the next pulse is applied to the system. The value of the then set *repetition time* reflects the magnitude of T_1. The *repetition time* is now chosen to be about 10 to 20 times the value. Fine tuning is done so that the FID does not change when the *repetition time* is changed.

6.3 Determination of T_1

Now for T_1 the above described measurement curve is recorded, i.e. a pulse sequence of $\pi \to \tau \to \frac{\pi}{2}$ is applied. It should be noted that the measured values represent only the magnitude. Thus, the part of the measurement curve up to the zero crossing of the magnetization must be provided with a factor -1. The blanking function of the amplifier can be used for the measurement. However, care should be taken to ensure that a certain residual pulse is still retained, which should not be confused with the FID. The evaluation must include the determination of T_1 from the zero-crossing-point method, by an exponential fit and by the determination of the slope from a semi-logarithmic plot. The error calculation must include both, reading inaccuracies and the errors due to statistics. The values obtained by each method are compared and estimated which is more accurate.

6.4 Determination of T_2

To determine T_2, a pulse sequence is used as described above, i.e. $\frac{\pi}{2} \to \tau \to \pi \to \tau$. The B-pulse is applied several times and from the two methods (Carr-Purcell or Meiboom-Gill) the one that gives the better result is chosen. The result of the other method is qualitatively described and reasons are given why it was not used. On the spectrometer there is a simple switch (marked MG for Meiboom-Gill), which makes the transition from Carr-Purcell to Meiboom-Gill. The evaluation here is again done by an exponential fit and by determining the slope from the semi-logarithmic order. The error calculation again includes the reading inaccuracies and the errors due to the statistics.

7 Questions for self-check

- What are the meanings of the eigenvalues and eigenstates in the ideal 2-level spin system?
- We use NMR frequencies in the MHz range. Why do the electrons present not interfere in these experiments?
- What do the Bloch equations say, and how can they be solved?
- Why is it enough to measure the voltages induced in the pickup coil, although we are interested in the magnetizations?
- What is the effect of the pre-measurement with the conductor loop?
- How are the relaxation times T_1 and T_2 determined experimentally?
- How do the improved pulse sequences for measuring T_2 according to Carr-Purcell and Meiboom-Gill work?

8 Experiment protocol

Tasks for evaluation

- Determination of B_1 and $\tau_{\pi/2}$ by means of the conductor loop
- Estimation of T_1 from the repetition time
- Determination of T_1 from the pulse sequence by
  - Plot of the magnetization vs. waiting time
  - Zero crossing point method
  - Exponential fit (determination of U_0 necessary)
  - Half-logarithmic plot and slope evaluation
- Comparison of Carr-Purcell and Meiboom-Gill for T_2
- Determination of T_2 from the pulse sequence by
  - Plot of the magnetization vs. waiting time
  - Exponential fit (determination of U_0 necessary
  - Half-logarithmic plot and slope evaluation

The protocol must contain:

- Goal of the experiment (1 page max.)
- Operating principle and setup
- Task and conduction of the experiment
- Evaluation (quantitative, including error calculation)
- Discussion (explanation of differences, origin of errors, resulting effects of the evaluation methods)
- Summary

The required points in the protocol and evaluation can be suitably combined and summarized in the text. The protocol should not contain:

- repetitive explanations from the text of the test instructions
- superfluous descriptions of the test procedure or information on test conditions which do not contribute significantly to the measurement result.

References

[1] C. P. Slichter, Principles of Magnetic Resonance (Springer Berlin Heidelberg, 1990).

[2] H. Y. Carr and E. M. Purcell, Phys. Rev. **94**, 630 (1954).

[3] S. Meiboom and D. Gill, Review of Scientific Instruments **29**, 688 (1958).